XLI CILAMCE
XLI Ibero-Latin American Congress on Computational Methods in Engineering
16-19 November, 2020 FOZ DO IGUAÇU PARANÁ - BRAZIL

Computational analisys of the Anterior Cruciate Ligament when climbing a step

Ing. C. Díaz-Cuadro[1], Dr. Ing. H. Figueredo[1], MSc. D. Santos[2]

[1]*Instituto de Ingeniería Mecánica y Producción Industrial, Facultad de Ingeniería, UdelaR,*
J. Herrera y Reissig 565, 11300, Montevideo, Uruguay
cdiaz@fing.edu.uy, henryf@fing.edu.uy
[2]*Departamento de Rehabilitación, Facultad de Medicina, UdelaR*
Avda. Italia, 11600, Montevideo, Uruguay
dsantos@hc.edu.uy

Abstract. The human body is a complex mechanic structure and the knee joint (KJ) is one of the most complex and demanded joint due to it has to carry very high loads and his structure must to enable triaxial movements without lose both, the stability and the control motor. In addition, the Anterior Cruciate Ligament (LCA) deficiency is one of the most common injuries of the KJ and affect about one of 3000 people in US every year. Moreover, a LCA deficiency commonly leads to more than one causes that produces articular surfaces damage or osteoarthritis. Many studies about the KJ had been carried out in both in-vivo and in-vitro and it showed a high variability by both person and age.

The aim of this work is to take a first step towards developing a procedure to quantify the subject specific LCA health with a non-invasive technique. This procedure is based on two steps, the motion capture and then the numeric simulation with the finite element method. For the motion capture we designed an experiment of climbing a step, to record the movements of the KJ with stereophotogrammetry using the well-known protocol Plug-in Gait developed by Vicon Motions Systems. We record the trajectories of the markers placed over the skin of the patient lower limb and extracted the curves of the knee kinematics. This data was transform to extract both, the flexion-extension an internal-external rotation curves, to use as boundary condition for the finite element model of the patient's tibiofemoral joint.

On the second part, we developed a 3D finite element model of the KJ starting from the model released by the OpenKnee project to run on FEBio. With this model we analyze the resulting joint kinematics and its changes when using, another constitutive models for the ligaments or different the mesh densities for de ACL. Moreover, we determine the kinematics of the LCA and the stress and strain distribution on this complex structure when climbing a step. The obtained results were compared against available data from literature and showed a good agreement. Furthermore, this procedure enable to work on the study of specific mechanic properties of soft tissues for each patient with this protocol as starting point in order to obtain more reliable results.

Keywords: Knee Joint, Motion Capture, FEM

1 Introduction

The human body is a complex mechanic structure and the knee joint (KJ) is one of the most complex and demanded joint due to it has to carry very high loads and his structure must to enable triaxial movements without lose both, the stability and the control motor [1]. In addition, the Anterior Cruciate Ligament (ACL) deficiency is one of the most common injuries of the KJ and affect about one of 3000 people in US every year [2]. Besides the scientific progress of the last fifty years, the long-term outcome of the ACL injury show a degradation of the articular kinematics wich could leads to early Osteoarthritis (OA). Therefore, increase the knowledge about, the behavior of the KJ and, the function and mechanic properties of each of their structures, to improve treatments [3–10].

Many studies about the KJ had been carried out in both in-vivo and in-vitro and it showed a high variability by both person and age [11–14]. Therefore, it is also needed the development of new techniques that allow to

evaluate the behavior of the KJ, and in particular, of the LCA and its reconstruction, with as less as possible effects on the patient.

Following the aforementioned paths, the aim of this work is to take a first step towards developing a procedure to quantify the subject specific LCA health with a non-invasive technique. In this work, we focus on figure out how to obtain the KJ kinematics data, and what could be the scope of this approach. However, is beyond the scope of this work, the subject-specific properties and geometries of each structure of the KJ, since we use generic data for this purpose.

To answer the previous questions, we propose a procedure based on two steps that we present in the next section, firstly we show the method to motion capture of the kinematics, and then we explain how the numeric simulation with the finite element method (FEM) was done.

2 Materials and Methods

The first stage, which is used as input in the Finite Element (FE) computational model, is the data preparation and it is composed by three tasks; The motion capture, the geometry determination, and the selection of the material model of the ligaments and bones (see Fig. 1). Then, the second stage is the finite element model of the knee joint with all the pre-processed data and analyze the outputs.

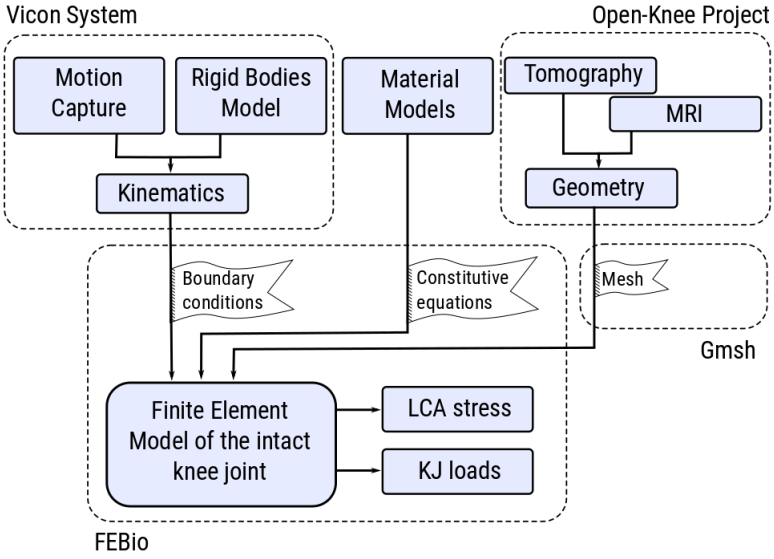

Figure 1. Flowchart of the procedure developed.

2.1 Motion capture

To obtain the KJ kinematics we use the gait laboratory of the Hospital de Clínicas (Montevideo, Uruguay) equipped with a Vicon System to make a stereophotogrammetry study. This task consists in record with eight synchronized cameras the movement of a patient, while he have reflective makers on specific places over the skin (see Fig. 2).

The Vicon System allows to obtain the 3D trajectories of each marker, composing the videos of eight cameras, with high precision. Moreover, if a loaded protocol is used, it will work taking into account others relations and restrictions that will be useful to determine important variables such as, joint rotation centers, joint angles, center of mass, among others.

In this case, it was used the modified *Plug-in Gait* protocol for lower limb (mPiG). This protocol determine the exact position of each marker over the patient skin and was developed by Vicon to evaluate the gait of a patient.

Figure 2. Left: Markers location over the patient - Right: Patient climbing the step.

The mPiG model consists in seven structures, which represent the pelvis, femur (x2), tibia (x2), and foot (x2), and six spherical joint that allow three Degrees of Freedom (DoF), which play the role of real joints. Although the real human joints are much more complex than a spherical joints because it have 6 DoF instead of 3, the translation DoF are neglected with this model taking into account that they have the same order that the error of motion capture.

The voluntary was a 50 years old man, without previous pathologies in regards to the knee joint, and with a height of $172cm$. Once finished to put all the 20 markers on the right location [15], we asked the voluntary for to repeat the task of climbing the step of the Fig. 2 ten times as similar as possible, while he was been recording with the Vicon System.

NEXUS is a VICON's software that process all the data obtained from the cameras while it impose the constrains and relations of the mPiG model to get the optimal solution for the data set. NEXUS solves an optimization problem in which it find the position of each rigid element (bones) for each frame, minimizing the error between the recorded position of all the markers and the most likely location of it, without breaking any constraint. Once it have the location of the bones for the whole time, is possible to determine the joint angles for each joint, and in particular for the right knee joint, which we use in this work. In Figure 3 can be seen the value of the angles of Flexo-Extension (FE), Internal-External Rotation (IE), and Varum-Valgum Rotation (VV) for the time of the ten repetition of the motor task.

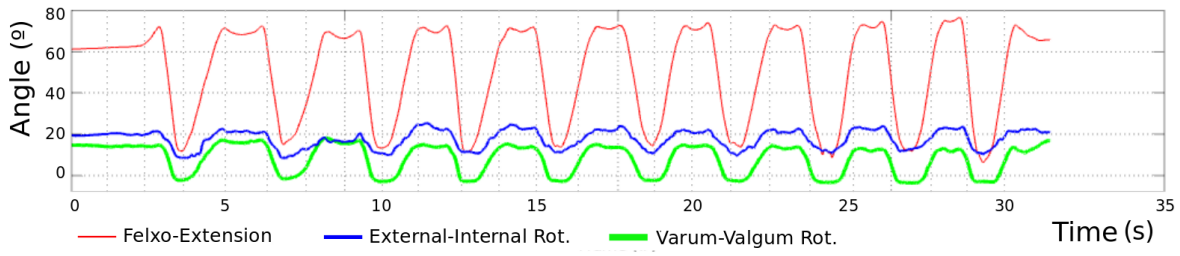

Figure 3. Angles of the knee joint.

Figure 3 show a high range of Varum-Valgum motion in contrast to the that can be found on literature, in fact, the common range for this parameter is $12^o \pm 2^o$ (see [5, 16]). This shows a clearly overestimation of the VV angle that can be attributed to cross-talk or Soft Tissue Artifact (see [17–21]). Therefore we do not use this curve for the boundary condition.

2.2 Geometry

In this work was used the geometry shared by the Open Knees Project [22, 23], which provide open access to 3D FE representation of the knee joint to investigation, development and experimentation to enlarge te knowledge on this topic. Specifically, the "*Generation 1*" was the representation used for this study, which comes from processed Magnetic Resonance Imagining (MRI). The Open Knees team created eleven independent structures, from the MRI in format *.iges* and that are; Femur, Tibia, Femoral cartilage, Tibial cartilage (x2), Cruciate Ligaments (x2), Collateral Ligaments (x2), and Menisci (x2). However, since the aim of this work is the LCA analysis, we only took into account the structures which interact with this ligament. In addition, the boundary condition are kinetics (no external force acting) the structures which we are not interested on, not need to be incorporated. This aspects leads to a simplification of the 11 structures-system to a 4 structure-system containing: Femur, Tibia, LCA and Posterior Cruciate Ligament (PCL).

2.3 Materials

Bones: It was decided to model this structures as rigid bodies, which means it can not be deformed. Although the bones are non-rigid bodies, when their strain is compared with that of the ligaments, the deformation that belong to the bones is negligible, and then can be assumed as a rigid bodies.

Ligaments: As a soft tissues, the ligaments presents a relationship between their stress and strain. In the case of ligaments and tendons there is a consensus in that they have to be modeled as Transversely Isotropic Hiperelastic (TIH) structures because of its nature of fibril reinforced materials. Its main direction, in which are stiffer than the others, is the longitudinal direction. *Weiss et al.* in 1996 [24] developed the Strain Energy Density (Ψ) for this type of material, starting by separate the matrix substance energy from the fibers' energy, as it is shown in Eq. 1.

$$\Psi(\mathbf{C}, a^0) = \Psi^m(\mathbf{C}) + \Psi^f(\mathbf{C}, a^0) \tag{1}$$

Where: $\mathbf{C}$ is the Right Cauchy Strain Tensor, and a^0 is the orientation of the fibers in reference configuration. Assuming the behavior of the matrix substance can be modeled as Mooney-Rivlin material we have the Eq. 2, in which, C_1 and C_2 are material's constants, K is the bulk modulus and I_i is the i^{th} invariant of $\mathbf{C}$:

$$\Psi^m(\mathbf{C}) = C_1(\widetilde{I}_1 - 3) + C_2(\widetilde{I}_2 - 3) + \frac{K}{2} ln(\sqrt{I_3})^2 \tag{2}$$

To determine the functional form of the term Ψ^f of the Eq. 1, *Weiss* in 1995 [25] made some experiments and concluded that the ligaments' fibers should have a Strain Energy Desity that follow the behavior showed in Eq. 3, considering $\lambda = L/L_0$ as the fiber's strech:

$$\lambda \frac{\partial \Psi^f}{\partial \lambda} = \begin{cases} 0, & \lambda < 1 \\ C_3 \left(e^{C_4(\lambda - 1)} - 1 \right), & 1 < \lambda < \lambda^* \\ C_5 \lambda + C_6, & \lambda > \lambda^* \end{cases} \tag{3}$$

Where C_3, C_4, and C_5 are material's constants and λ^* is the stretched in which all the fibers are recruited and start the linear behavior.

As can be seen in Eqs. 2 and 3 this material model needs seven parameters which in this study are used the same that *Peña et al.* used in [12, 26, 27] (see Table 1).

To compare the results of the TIH model and to analyze the repercussion of the addition of the fibers into the model of the ligaments, we also used another model to simulate the case in which the ligaments were only the matrix substance. To do that, we used the Neo-Hookean (N-H) Strain Energy Density as a material model for the ligaments, with the same C_1 and K constants of the Table 1.

Table 1. Properties of the LCA and the PCL for the HTI model extracted from [12]

	$C_1(MPa)$	K	$C_2(MPa)$	$C_3(MPa)$	C_4	$C_5(MPa)$	λ^*
LCA	1,95	73,21	0	0,0139	116,22	535,039	1,046
LCP	3,25	121,95	0	0,1196	87,178	431,036	1,035

2.4 Mesh and simulation

The discretization of the geometry was done with the 3D mesh generator Gmsh [28], which allows to select both, the element size and where to refine the mesh. This tool is useful since the Finite Element Method theory establishes that the solution of the computational method tends to the exactly solution when the element size decrease. However, while increase the number of elements also do it the time consumption. Therefore, it is necessary to find a midpoint between time and resolution. For this case, we found that a acceptable resolution of the results is reached with the number of elements that can bee see in Table 2 for each structure, with a reasonable time of computing. Moreover, also can be seen the refinement of bones and ligaments in Fig. 4.

Table 2. Parámetros de mallado de cada estructura

	Form	Nodes	Quantity	Average volume (mm^3)
Femur	tetrahedra	4	15.759	8.6
Tibia	tetrahedra	4	9.297	8.2
ACL	tetrahedra	10	146.442	0.003
PCL	tetrahedra	4	28.159	0.025

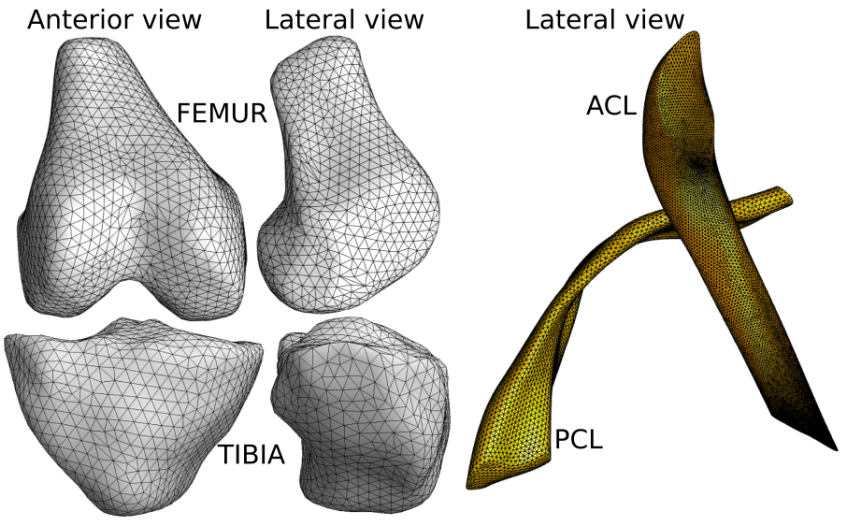

Figure 4. Discretization of the 4 structures

Once all the previous step are completed the next is to setup the simulations. To do that we used the software FEBio [29] which is a nonlinear finite element solver that is specifically designed for biomechanics and biophysics applications.

3 Results and Discussion

The simulation of the two cases was done on a computer with the following characteristics: Processor Intel i5-7400 CPU @ 3.00GHz-x4 and 16GB de RAM and the time consumption was near to 8 hours each.

In Figure 5 can be seen the principal stress distribution for the KJ with the TIH ligament model at the moment of the most critical situation, wich is when at $0.25s$ started the ascent.

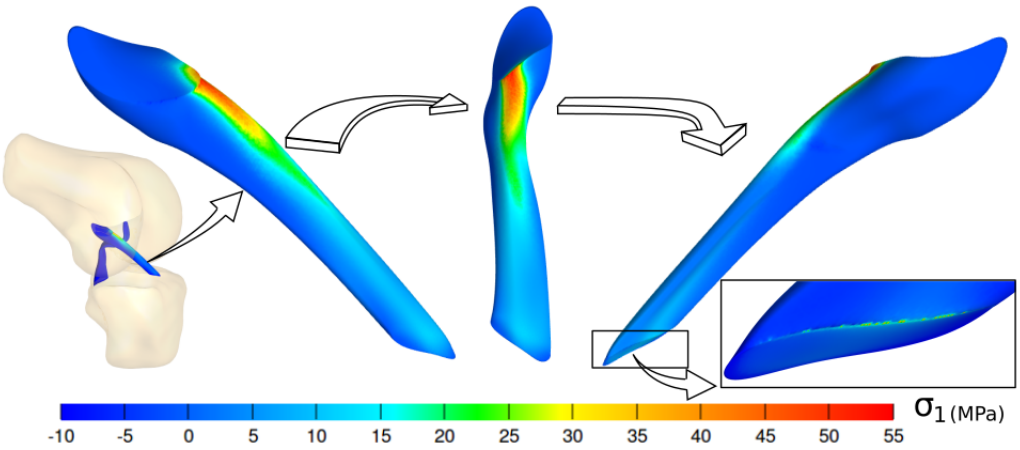

Figure 5. Most critical principal stress distribution on the ACL modeled with HTI.

On the left of Fig. 5 can be seen the position of the KJ at $0.25s$ of ascent and then, in the middle the image shows that the most critical zone on the ACL is the anterior part, near to the femoral attach, in the anterior part, which agreed with the literature [8, 30, 31]. Furthermore, the maximum principal stress reached $52MPa$ that also match with the range presented in [12] and [32], in which similar situations are tested.

In addition, on the right of Fig. 5 we present a detail of the posterior zone of the tibial ACL attach, where can be seen some high values compared to those around. This occur because that zone have geometrical and material discontinuities since is the transition between a soft tissue (ligament) and a rigid body (tibia). This gradients cause high stress values that could be not realistic, because in real KJ there are a more gradual transitions on this zones.

Next we determined the loads that the femur has to defeat to do the prescribed movement. That loads, which are torques and forces generated by the ligaments as a response of their deformation, are shown in Feg. 6.

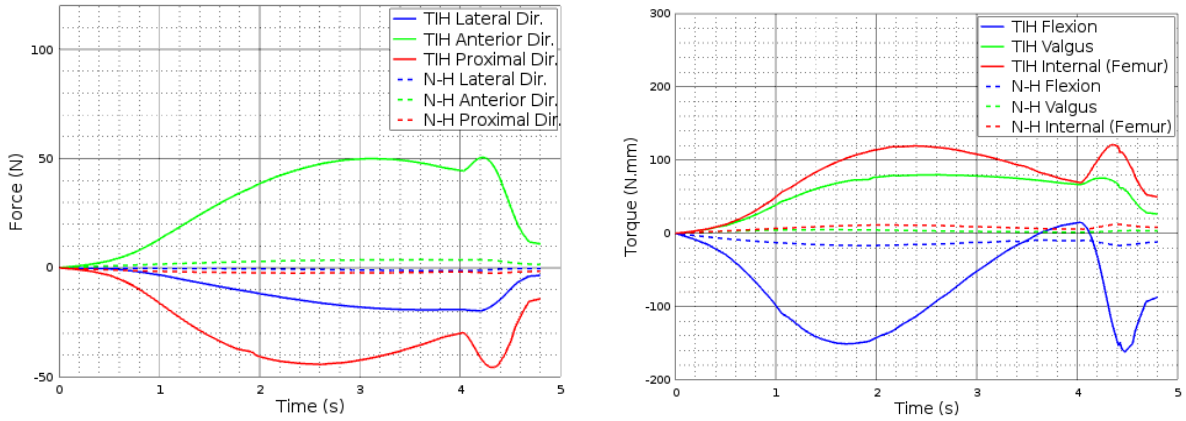

(a) Forces on the femur.

(b) Torques on the femur.

Figure 6. Loads on the bones generated by the ligaments.

Considering the fact that during flexion the PCL is slack, the forces that it can perform are negligible com-

pared to those of the ACL, which is tightened. Therefore, all the loads that can be seen in Fig. 6 are developed almost entirely by the ACL. In Fig. 6(a) we can observe that the femur is mainly forced in the tibial direction keeping the bones together (red curve) and in the anterior direction constraining the posterior translation of the femur (green curve). The femur is secondly forced to the medial direction. This results agreed with the ACL direction, and with one of the mainly ACL function which is to avoid the tibia anterior translation. Besides, both simulations (TIH and N-H) have the same trends, there is a clearly high difference between each pair of curves, evidencing the important of simulating the fibers of the ligaments.

In Figure 6(b) we also can see the torques on the femur and worth to note that the movement is mainly constrained in the flexion at its first degrees but then decrease quickly. That is likely because despite the increase of the force, the moment arm, in regards of the joint rotation center, decrease. To a lesser extent the external and varus rotations are also constrained by the action of the ACL, which agree with other of the functions of this ligament [10]..

4 Conclusions

Firstly, we come up with a procedure that allows the use of experimental data of motion capture on a FE generic model, but in order to use subject-specific material properties and geometry, in near future. This work also show that the results obtained with this steps reach similar results than other works [8, 12, 30–33], which indicate that could be a novel way to asses the state of the KJ health.

Secondly, we presented the importance in correct use of the ligaments' properties, because the result are highly sensitive to this parameters. The difference is quite considerably between models than use only the stiffness of the matrix substance and those which also consider the fibers' stiffness.

Finally, this work allows to determine the loads that the ACL is subject when a patient climbing a step from the motion capture of this motor task. However, it was assumed that the translation DoF of the knee are negligible since they are not considering in the mPiG model. That is necessary to verify with other models before go on this procedure.

Authorship statement. The authors hereby confirm that they are the sole liable persons responsible for the authorship of this work, and that all material that has been herein included as part of the present paper is either the property (and authorship) of the authors, or has the permission of the owners to be included here.

References

[1] Trad, Z., Barkaoui, A., Chafra, M., & Tavares, J. M. R., 2018. *FEM analysis of the human knee joint: a review*. Springer.

[2] Kim, S., Bosque, J., Meehan, J. P., Jamali, A., & Marder, R., 2011. Increase in outpatient knee arthroscopy in the united states: a comparison of national surveys of ambulatory surgery, 1996 and 2006. *JBJS*, vol. 93, n. 11, pp. 994–1000.

[3] Dienst, M., Burks, R. T., & Greis, P. E., 2002. Anatomy and biomechanics of the anterior cruciate ligament. *The Orthopedic clinics of North America*, vol. 33, n. 4, pp. 605–20.

[4] Girgis, F. G., Marshall, J. L., & Monajem, A., 1975. The cruciate ligaments of the knee joint. anatomical, functional and experimental analysis. *Clinical orthopaedics and related research*, , n. 106, pp. 216–231.

[5] Jakob, R. P. & Stäubli, H., 1992. *The Knee and the cruciate ligaments: anatomy, biomechanics, clinical aspects, reconstruction, complications, rehabilitation*. Springer.

[6] Mallett, K. F. & Arruda, E. M., 2017. Digital image correlation-aided mechanical characterization of the anteromedial and posterolateral bundles of the anterior cruciate ligament. *Acta biomaterialia*, vol. 56, pp. 44–57.

[7] Marieswaran, M., Jain, I., Garg, B., Sharma, V., & Kalyanasundaram, D., 2018. A review on biomechanics of anterior cruciate ligament and materials for reconstruction. *Applied bionics and biomechanics*, vol. 2018.

[8] McLean, S. G., Mallett, K. F., & Arruda, E. M., 2015. Deconstructing the anterior cruciate ligament: what we know and do not know about function, material properties, and injury mechanics. *Journal of biomechanical engineering*, vol. 137, n. 2.

[9] Noyes, F. R., DeLucas, J. L., & Torvik, P. J., 1974. Biomechanics of anterior cruciate ligament failure: An analysis of. *J. Bone Joint Surg. Am*, vol. 56, pp. 236–253.

[10] Siebold, R., Dejour, D., & Zaffagnini, S., 2014. *Anterior cruciate ligament reconstruction: a practical surgical guide*. Springer Science & Business.

[11] Naghibi Beidokhti, H., 2018. *Personalized Finite element models of the knee joint: a platform for optimal orthopedic surgery pre-planning*. PhD thesis, [Sl: sn].
[12] Pena, E., Calvo, B., Martinez, M., & Doblare, M., 2006. A three-dimensional finite element analysis of the combined behavior of ligaments and menisci in the healthy human knee joint. *Journal of biomechanics*, vol. 39, n. 9, pp. 1686–1701.
[13] Marra, M., 2019. *Personalized musculoskeletal modeling of the knee joint*. PhD thesis, [Sl: sn].
[14] Shu, L., Yamamoto, K., Yao, J., Saraswat, P., Liu, Y., Mitsuishi, M., & Sugita, N., 2018. A subject-specific finite element musculoskeletal framework for mechanics analysis of a total knee replacement. *Journal of biomechanics*, vol. 77, pp. 146–154.
[15] VICON, 2005. Pig advances notes, concepts and kinematics.
[16] Chhabra, A., Elliott, C. C., & Miller, M. D., 2001. Normal anatomy and biomechanics of the knee. *Sports medicine and arthroscopy review*, vol. 9, n. 3, pp. 166–177.
[17] Chiari, L., Della Croce, U., Leardini, A., & Cappozzo, A., 2005. Human movement analysis using stereophotogrammetry: Part 2: Instrumental errors. *Gait & posture*, vol. 21, n. 2, pp. 197–211.
[18] Leardini, A., Chiari, L., Della Croce, U., & Cappozzo, A., 2005. Human movement analysis using stereophotogrammetry: Part 3. soft tissue artifact assessment and compensation. *Gait & posture*, vol. 21, n. 2, pp. 212–225.
[19] Andersen, M. S., Benoit, D. L., Damsgaard, M., Ramsey, D. K., & Rasmussen, J., 2010. Do kinematic models reduce the effects of soft tissue artefacts in skin marker-based motion analysis? an in vivo study of knee kinematics. *Journal of biomechanics*, vol. 43, n. 2, pp. 268–273.
[20] Charlton, I., Tate, P., Smyth, P., & Roren, L., 2004. Repeatability of an optimised lower body model. *Gait & Posture*, vol. 20, n. 2, pp. 213–221.
[21] Stief, F., B¨ohm, H., Michel, K., Schwirtz, A., & D¨oderlein, L., 2013. Reliability and accuracy in three-dimensional gait analysis: a comparison of two lower body protocols. *Journal of applied biomechanics*, vol. 29, n. 1, pp. 105–111.
[22] Erdemir, A. & Sibole, S., 2010. Open knee: a three-dimensional finite element representation of the knee joint. *User's guide, version*, vol. 1, n. 0.
[23] Erdemir, A., 2013. Open knee: a pathway to community driven modeling and simulation in joint biomechanics. *Journal of medical devices*, vol. 7, n. 4.
[24] Weiss, J. A., Maker, B. N., & Govindjee, S., 1996. Finite element implementation of incompressible, transversely isotropic hyperelasticity. *Computer methods in applied mechanics and engineering*, vol. 135, n. 1-2, pp. 107–128.
[25] Weiss, J. A., 1995. A constitutive model and finite element representation for transversely isotropic soft tissues.
[26] Weiss, J. A., Gardiner, J. C., & Bonifasi-Lista, C., 2002. Ligament material behavior is nonlinear, viscoelastic and rate-independent under shear loading. *Journal of biomechanics*, vol. 35, n. 7, pp. 943–950.
[27] Łuczkiewicz, P., Daszkiewicz, K., Witkowski, W., Chróścielewski, J., & Zarzycki, W., 2015. Influence of meniscus shape in the cross sectional plane on the knee contact mechanics. *Journal of biomechanics*, vol. 48, n. 8, pp. 1356–1363.
[28] Geuzaine, C. & Remacle, J.-F., 2009. Gmsh: A 3-d finite element mesh generator with built-in pre-and post-processing facilities. *International journal for numerical methods in engineering*, vol. 79, n. 11, pp. 1309–1331.
[29] Maas, S. A., Ellis, B. J., Ateshian, G. A., & Weiss, J. A., 2012. Febio: finite elements for biomechanics. *Journal of biomechanical engineering*, vol. 134, n. 1.
[30] Butler, D. L., Guan, Y., Kay, M. D., Cummings, J. F., Feder, S. M., & Levy, M. S., 1992. Location-dependent variations in the material properties of the anterior cruciate ligament. *Journal of biomechanics*, vol. 25, n. 5, pp. 511–518.
[31] Bonnin, M., Amendola, N. A., Bellemans, J., MacDonald, S. J., & Menetrey, J., 2013. *The knee joint: surgical techniques and strategies*. Springer Science & Business Media.
[32] Fernandes, D. J. C., 2014. Finite element analysis of the acl-deficient knee. *Lisbon: University of Lisbon*.
[33] Pena, E., Martinez, M., Calvo, B., Palanca, D., & Doblare, M., 2005. A finite element simulation of the effect of graft stiffness and graft tensioning in acl reconstruction. *Clinical Biomechanics*, vol. 20, n. 6, pp. 636–644.